Received: 1 June 2018 | Revised: 19 July 2018 | Accepted: 30 August 2018

DOI: 10.1002/navi.278

ORIGINAL ARTICLE

WILEY ION

A regression-based methodology to improve estimation of inertial sensor errors using Allan variance data

Juan Jurado | Christine M. Schubert Kabban | John Raquet

Air Force Institute of Technology, Wright-Patterson AFB, Dayton, Ohio, 45433

Correspondence
Juan Jurado, Air Force Institute of Technology, Wright-Patterson AFB, Dayton, OH 45433.
Email: juan.jurado@afit.edu

Funding information
Air Force Institute of Technology

Abstract

This research proposes a novel, autonomous, regression-based methodology for Allan variance analysis of inertial measurement unit (IMU) sensors. Current methods for Allan variance analysis have been rooted in the human-based interpretation of linear trends, referred to as the slope method. The slope method is so prolific; it is referenced among electrical and electronics engineering standards for IMU error analysis. However, the graphical nature and visual-inspection–based use of the method limit its ability to be programmed as a generalized algorithm, which hinders the autonomy desired in modern-day navigation computations. Using nonlinear regression with a ridge-regression initial guess, the proposed method is shown to produce comparable results to the gold standard slope method when using standard-length data collections and outperforms the slope method when the amount of available data is limited. This development directly enables accurate navigation solutions for all vehicles in land, air, sea, and space operations.

1 | INTRODUCTION

Inertial navigation systems are used to track the location and velocity of an object and are relied upon commonly by many vehicles as a means of establishing orientation in open spaces such as ships in the ocean and airplanes in the sky. However, the availability of an accurate inertial navigation solution depends on the proper calibration of the deterministic and stochastic errors associated with the accelerometers and gyroscopes that compose the inertial measurement unit (IMU). Without proper quantification of their deterministic and stochastic errors, the solutions rendered by the IMU-based upon accelerometer and gyroscope measurements are subject to drift and are, at best, erroneous, and at worst, provide fatal navigation information. As such, a considerable amount of time and energy has been invested in the understanding and modeling of the various sources of noise that affect the components of the IMU. Adequate modeling of inertial sensor errors begins with an understanding of the physical processes from which deterministic and stochastic errors arise. In general, any given sensor output signal can be written in the following form:

$$\mathbf{y}_k = \mathbf{M}\mathbf{x}_k + \boldsymbol{\epsilon}_k, \tag{1}$$

where $\mathbf{y}_k$ is the measured output signal, $\mathbf{x}_k$ is the true signal, $\mathbf{M}$ is a linear operator on $\mathbf{x}_k$, and $\boldsymbol{\epsilon}_k$ is an additive, possibly nonlinear signal composed of a combination of stochastic and deterministic errors that vary with sensor type. For inertial sensors, the majority of existing research adapts a version of (1) to both accelerometers and gyroscopes by providing specific forms of $\mathbf{M}$ and further refining the deterministic components and stochastic processes governing $\boldsymbol{\epsilon}_k$.

Titterton[1] provides general error models for gyroscopes and accelerometers in order to describe a wide array of deterministic and stochastic errors. For gyroscopes, the

relationship between true (ω_x) and measured ($\tilde{\omega}_x$) angular rate for a single axis x is given by the following:

$$\begin{aligned}\tilde{\omega}_x = (1+S_x)\omega_x + M_y\omega_y + M_z\omega_z + B_{fx} \\ +B_{gx}a_x + B_{gz}a_z + B_{axz}a_xa_z + \eta_x,\end{aligned} \tag{2}$$

where S_x is the x-axis scale factor, M_y and M_z are cross coupling coefficients, B_{fx} is a constant x-axis bias (non g-sensitive), B_{gx} and B_{gz} are g-sensitive bias coefficients along the input and spin axes, B_{axz} is the anisoelastic bias coefficient, and η_x is zero-mean additive white Gaussian noise. It is important to note that the previously discussed terms may be deterministic or stochastic in nature. Most often, such terms are modeled as correlated stochastic processes that eventually motivate the need for a reliable stochastic characterization method such as the Allan variance.[2] The expanded form in (2) can be applied to the remaining two axes and expressed in terms of (1) by letting

$$\mathbf{y} = \begin{bmatrix}\tilde{\omega}_x \\ \tilde{\omega}_y \\ \tilde{\omega}_z\end{bmatrix} \qquad \mathbf{x} = \begin{bmatrix}\omega_x \\ \omega_y \\ \omega_z\end{bmatrix}, \tag{3}$$

$$\mathbf{M} = \begin{bmatrix}1+S_x & M_y & M_z \\ M_x & 1+S_y & M_z \\ M_x & M_y & 1+S_z\end{bmatrix}, \tag{4}$$

$$\boldsymbol{\epsilon} = \begin{bmatrix}B_{fx} + B_{gx}a_x + B_{gz}a_z + B_{gxz}a_{xz} + \eta_x \\ B_{fy} + B_{gy}a_y + B_{gx}a_x + B_{gyx}a_{yx} + \eta_y \\ B_{fz} + B_{gz}a_z + B_{gy}a_y + B_{gzy}a_{zy} + \eta_z\end{bmatrix}. \tag{5}$$

Similarly,[1] Titterton and Weston also describe a general error model for accelerometers in terms of the relation between true (a_x) and measured ($\tilde{a}_x$) acceleration for a single axis x as follows:

$$\tilde{a}_x = (1+S_x)a_x + M_ya_y + M_za_z + B_f + B_va_xa_y + \eta_x, \tag{6}$$

where S_x is the x-axis scale factor, M_y and M_z are cross coupling coefficients, B_f is a constant measurement bias, B_v is the vibro-pendulus error coefficient, and η_x is zero-mean additive white Gaussian noise. Again, (6) can be expressed using the form in (1) by letting

$$\mathbf{y} = \begin{bmatrix}\tilde{a}_x \\ \tilde{a}_y \\ \tilde{a}_z\end{bmatrix} \qquad \mathbf{x} = \begin{bmatrix}a_x \\ a_y \\ a_z\end{bmatrix}, \tag{7}$$

$$\mathbf{M} = \begin{bmatrix}1+S_x & M_y & M_z \\ M_x & 1+S_y & M_z \\ M_x & M_y & 1+S_z\end{bmatrix}, \tag{8}$$

$$\boldsymbol{\epsilon} = \begin{bmatrix}B_f + B_va_xa_y + \eta_x \\ B_f + B_va_ya_z + \eta_y \\ B_f + B_va_za_y + \eta_z\end{bmatrix}. \tag{9}$$

Subtle differences in $\mathbf{M}$ and $\boldsymbol{\epsilon}$ are found throughout literature based on the technology used in sensor development (ie, mechanical and ring laser). Although such differences affect the specific set of parameters found in $\mathbf{M}$, in general, all models for gyroscopes and accelerometers can be expressed as an adaptation of (1), with $\boldsymbol{\epsilon}$ composed of a common mixture of deterministic and stochastic terms. Focusing on such terms, Kirkko-Jaakkola et al[3] use a form similar to (1) and describe three types of stochastic gyroscopic errors in $\boldsymbol{\epsilon}$ as "constant bias, uncorrelated white noise, and $1/f$ (flicker) noise." Similar terms appear along with additional sources of error in Hou,[4] where a common set of five error sources are modeled using the "Allan variance slope method."[2,5,6] Although many stochastic modeling and calibration methods have been developed, the "Allan variance slope method" is commonly used in the navigation community and is listed as the method of choice in IMU error analysis standards.[7] As such, this research focuses on improving the mathematical methods for autonomously analyzing Allan variance data in the context of IMU calibration.

2 | ALLAN VARIANCE

Having established the importance of properly modeling the sources of noise in $\boldsymbol{\epsilon}$, we now turn to the most commonly used method for doing so found in literature, the Allan variance.[2] It is important to note that although common, the Allan variance is not the only existing method of IMU characterization. Other methods based on power spectral density (PSD) and autocorrelation function (ACF),[4,5] as well as wavelet-based methods,[8-10] are often used when analysis of complex signals is inadequate with the Allan variance (eg, when the signal is composed of more than one latent correlated noise process). Nevertheless, the Allan variance was originally developed for the analysis of error sources in atomic clocks. Later, it was found useful for identifying error sources in accelerometers and gyroscopes using a "slope method" for analyzing the Allan variance measurements. Such use of the Allan variance in IMU modeling is so prolific across literature that it was compiled into an Institute of Electrical and Electronics Engineers (IEEE) standard.[7] In general, the Allan variance, $\sigma_a^2(\tau)$, of a continuous time signal, $\Omega(t)$, is a function of a quantity called averaging time, τ, and is given by the following:

$$\sigma_a^2(\tau) = \frac{1}{2(N-2n)}\sum_{k=1}^{N-2n}\left[\bar{\Omega}_{k+1}(\tau) - \bar{\Omega}_k(\tau)\right]^2, \tag{10}$$

TABLE 1 Summary of Allan deviation slopes for common noise processes in IMU calibration

Error Source	Symbol	Relation to PSD	Graphical ID: Slope	Graphical ID: τ at desired σ	Coefficient Units[a]
Quantization	σ_q	$\sigma_a(\tau) = \sigma_q\sqrt{3}\tau^{-1}$	-1	$\sqrt{3}$	(deg) or (m/s)
Random Walk	σ_{rw}	$\sigma_a(\tau) = \sigma_{rw}\tau^{-1/2}$	$-1/2$	1	(deg/$\sqrt{\text{hr}}$) or (m/s/$\sqrt{\text{hr}}$)
Bias Instability	σ_b	$\sigma_a(\tau) = \sigma_b\sqrt{\frac{2\log(2)}{\pi}}\tau^0$	0	–	(deg/hr) or (m/s/hr)
Rate Random Walk	σ_{rrw}	$\sigma_a(\tau) = \sigma_{rrw}\frac{1}{\sqrt{3}}\tau^{1/2}$	1/2	3	(deg/hr/$\sqrt{\text{hr}}$) or (m/s/hr/$\sqrt{\text{hr}}$)
Rate Ramp	σ_{rr}	$\sigma_a(\tau) = \sigma_{rr}\frac{1}{\sqrt{2}}\tau^1$	1	$\sqrt{2}$	(deg/hr/hr) or (m/s/hr/hr)

[a] Units result from $\sigma(\tau)$ measured in deg/h or m/s/h and τ measured in hours.

$$n = \frac{\tau}{\Delta t}, \tag{11}$$

where N is the total number of samples in the discretized signal, Δt is the sampling period, and

$$\bar{\Omega}_k(\tau) = \frac{1}{\tau}\int_{t_k}^{t_k+\tau} \Omega(t)\mathrm{d}t, \qquad \Delta t \le \tau \le N\Delta t/2. \tag{12}$$

Essentially, (10) divides the sampled signal into clusters, $\bar{\Omega}_k(\tau)$, averaged over a duration, τ, and computes the variance among groups as a function of varying τ. It is important to note the form of (10) is referred to as "non-overlapping," since the clusters $\bar{\Omega}_k(\tau)$ do not overlap across time. Additionally, since each Allan variance point is computed from a finite set of samples per cluster, a percent error was derived in Papoulis and Pillai[11] and is given by the following:

$$\delta_a = \frac{1}{\sqrt{2\left(\frac{N}{n}-1\right)}}. \tag{13}$$

The Allan variance can then be equated to the PSD of the input signal using the following:

$$\sigma^2(\tau) = 4\int_0^\infty S_\Omega(f)\frac{\sin^4(\pi f\tau)}{(\pi f\tau)^2}\mathrm{d}f, \tag{14}$$

where f is frequency and $S_\Omega(f)$ is the PSD of $\Omega(t)$. The relationship illustrated in (14) is then used in Hou[4] and El-Sheimy et al[5] to exploit the properties of five key error sources: quantization, velocity/angle random walk, bias instability, acceleration/angular rate random walk, and rate ramp. Each of the five sources of error are systematically identified from an Allan variance plot of sensor (accelerometer or gyroscope) data using the slopes of the relationship between the PSD of each error source and its corresponding Allan variance formula. This relationship is explored in the following sections in order to develop an understanding of the slope method.

2.1 | Slope method

This section describes the prolific slope method of identifying the five aforementioned sources of accelerometer and gyroscope error using Allan variance analysis. As shown below, this method exploits the relationship between an error source's PSD and its corresponding Allan variance formula in a graphical context, whereby the slope of the Allan variance versus τ graph is visually analyzed in order to extract the necessary information to estimate error. Although this method is simple and generally accurate, it suffers from two main limitations. First, it is difficult to automate since it is rooted in human visual inspection of an Allan variance versus τ graph. As such, it requires complex logical programming or human intervention in the presence of nonstandard conditions (eg, missing sources of noise). Additionally, when the length of sensor data is incomplete (ie, not long enough to capture the underlying noise processes), the resulting Allan variance curve tends to become much more variable across data collections as τ increases. Such variability results in Allan variance slope behavior that is difficult to predict, making automated slope detection unreliable. Table 1 summarizes the key components of the slope method, while Figures 1 and 2 illustrate the process.

2.1.1 | Quantization error

Quantization is defined as the act of sampling an analog signal into discrete levels of size Δ during the analog-to-digital conversion process. The errors (differences between the analog signal and the digitized signal) caused by such quantization can be characterized as additive noise,[7,12] which is uniformly distributed between $-\Delta/2$ and $\Delta/2$. [7] Analyzing the relationship between the PSD function and the Allan deviation, $\sigma_a(\tau)$, of a signal composed only of quantization noise[4] gives the following:

$$\sigma_a(\tau) = \frac{\sigma_q\sqrt{3}}{\tau} = \sigma_q\sqrt{3}\tau^{-1}. \tag{15}$$

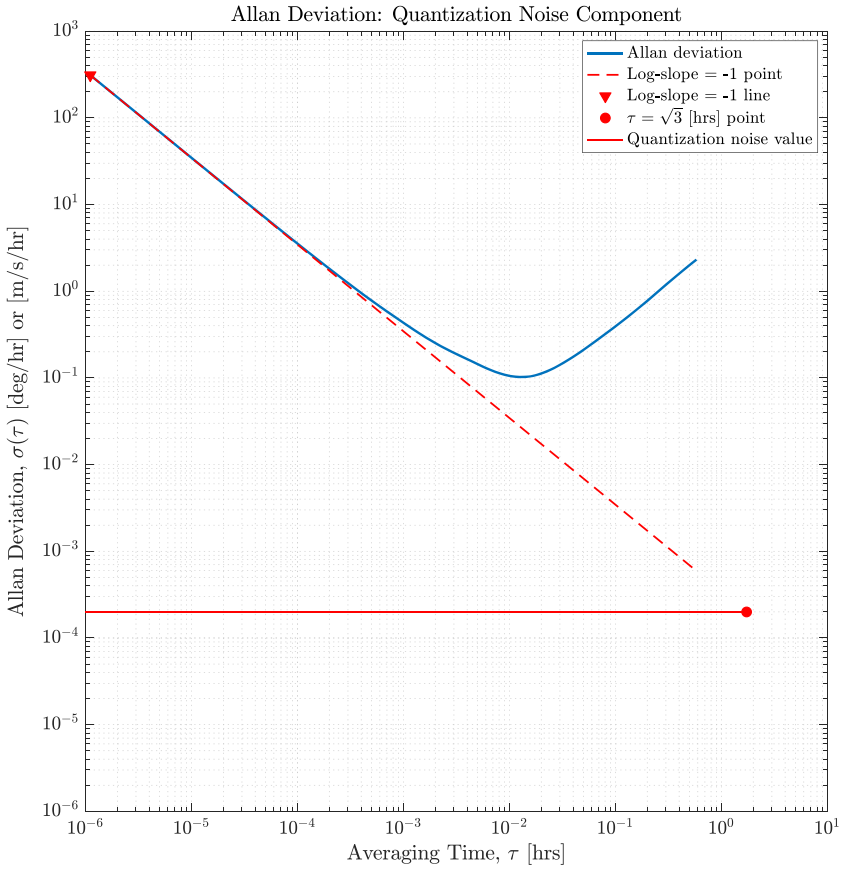

FIGURE 1 Illustration of Allan variance slope method for quantization noise [Color figure can be viewed at wileyonlinelibrary.com and www.ion.org]

Next, taking the common logarithm of both sides in (15) yields the following:

$$\log_{10}(\sigma_a(\tau)) = \log_{10}\left(\sigma_q\sqrt{3}\tau^{-1}\right) \tag{16}$$

$$= -\log_{10}(\tau) + \log_{10}(\sigma_q) + \log_{10}\left(\sqrt{3}\right), \tag{17}$$

which implies σ_q can be identified in an Allan deviation curve by finding a -1 slope when plotting $\log_{10}(\sigma_a(\tau))$ against $\log_{10}(\tau)$. Additionally, letting $\tau = \sqrt{3}$ in (17) solves the equation for σ_q, which means if the -1 slope line is projected to $\tau = \sqrt{3}$, the value of $\sigma_a(\tau)$ at that point will equal σ_q. This process is illustrated in Figure 1 and summarized in Table 1.

2.1.2 | Angle/velocity random walk

As indicated by its name, angle or velocity random walk is a random walk process observed in the angle or velocity signal output of an inertial sensor. In terms of (2) or (6), angle/velocity random walk arises from integrating η_x in $\tilde{\omega}_x$ or $\tilde{a}_x$. The relationship between the Allan deviation and the PSD for a signal of this type is given by the following:

$$\sigma_a(\tau) = \frac{\sigma_{rw}}{\sqrt{\tau}} = \sigma_{rw}\tau^{-1/2}. \tag{18}$$

Repeating the process followed for quantization noise yields the following:

$$\log_{10}(\sigma_a(\tau)) = \log_{10}(\sigma_{rw}\tau^{-1/2}) \tag{19}$$

$$= -\frac{1}{2}\log_{10}(\tau) + \log_{10}(\sigma_{rw}), \tag{20}$$

which implies σ_{rw} can be identified in an Allan deviation curve by finding a $-1/2$ slope when plotting $\log_{10}(\sigma_a(\tau))$ against $\log_{10}(\tau)$. Letting $\tau = 1$ in (20) solves the equation for σ_{rw}, which means if the $-1/2$ slope line is projected to $\tau = 1$, the value of $\sigma_a(\tau)$ at that point will equal σ_{rw}.

2.1.3 | Bias instability

Bias instability, sometimes referred to ironically as bias stability, refers to the tendency of an inertial sensor's constant bias (B_f in (2) or (6)) to change or drift during use. The most

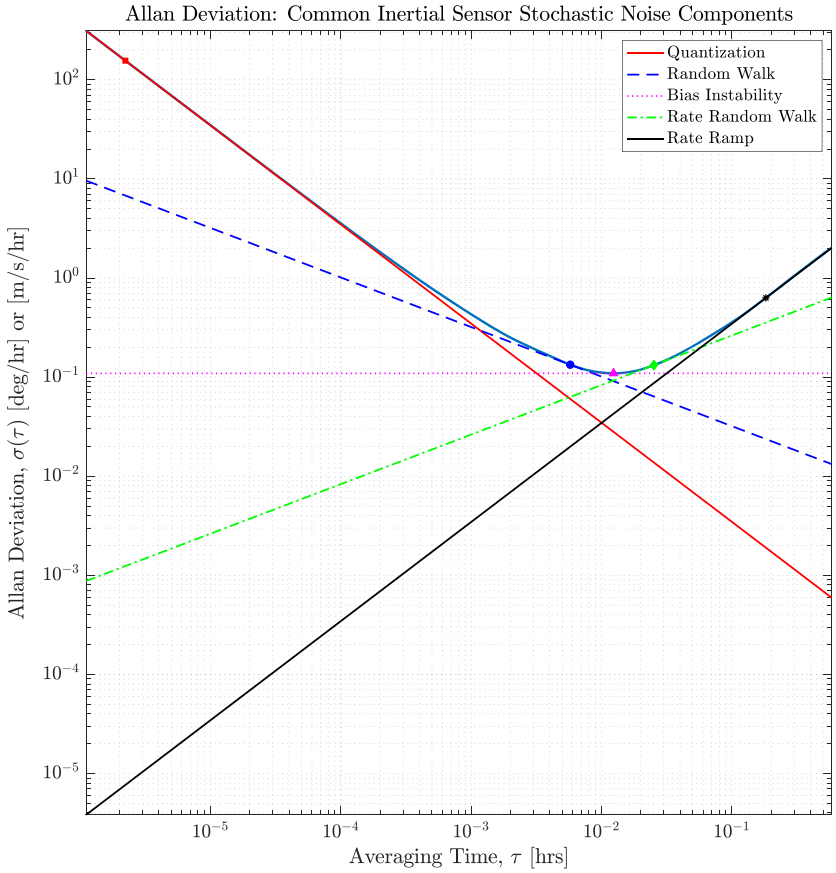

FIGURE 2 Illustration of Allan variance slope method for common stochastic noise components [Color figure can be viewed at wileyonlinelibrary.com and www.ion.org]

accurate description of the stochastic process behind this drift is flicker (or $1/f$) noise as shown by Kirkko-Jaakkola et al.[3] However, due to complications in the modeling of flicker noise in common navigation estimation algorithms, such as a Kalman filter,[13] this process is often approximated by a first-order Gauss-Markov process.[7,(figure C.6), 14] Following the slope method process yields the following:

$$\sigma_a(\tau) = \sigma_b \sqrt{\frac{2\log(2)}{\pi}} = \sigma_b \sqrt{\frac{2\log(2)}{\pi}} \tau^0, \tag{21}$$

$$\log_{10}(\sigma_a(\tau)) = 0\log_{10}(\tau) + \log_{10}(\sigma_b) + \log_{10}\left(\sqrt{\frac{2\log(2)}{\pi}}\right). \tag{22}$$

which indicates there is no relation to τ in (21). That is, the flicker noise coefficient can be identified in an Allan deviation curve by finding a 0 slope when plotting $\log_{10}(\sigma_a(\tau))$ against $\log_{10}(\tau)$. Additionally, (22) implies the value of $\sigma_a(\tau)$ at that point should be scaled by $\sqrt{2\log(2)/\pi}$ to solve for σ_b.

2.1.4 | Acceleration/angular rate random walk

In contrast to angle/velocity random walk, rate random walk refers to a random walk process observed in the inertial sensor's rate signal (acceleration or angular rate). In terms of (2) or (6), rate random walk arises from integrating white noise found in $\dot{\tilde{\omega}}_x$ or $\dot{\tilde{a}}_x$. Again, the relationship between the Allan deviation and the PSD for a signal of this type yields the following:

$$\sigma_a(\tau) = \sigma_{rrw} \sqrt{\frac{\tau}{3}} = \sigma_{rrw} \frac{1}{\sqrt{3}} \tau^{1/2}, \tag{23}$$

$$\log_{10}(\sigma_a(\tau)) = \frac{1}{2}\log_{10}(\tau) + \log_{10}(\sigma_{rrw}) - \frac{1}{2}\log_{10}(3), \tag{24}$$

which implies σ_{rrw} can be identified in an Allan deviation curve by finding a $+1/2$ slope when plotting $\log_{10}(\sigma_a(\tau))$ against $\log_{10}(\tau)$. Letting $\tau = 3$ in (24) solves the equation for σ_{rrw}, which means if the $+1/2$ slope line is projected to $\tau = 3$, the value of $\sigma_a(\tau)$ at that point will equal σ_{rrw}.

2.1.5 | Rate ramp

Finally, rate ramp refers to the deterministic, linear, and usually long-term increase of the inertial sensor's rate signal output. In terms of (2) or (6), rate random walk arises when B_{fx} or B_f linearly changes over time at a deterministic (eg, nonstochastic but unknown) rate. The slope method then yields the following:

$$\sigma_a(\tau) = \sigma_{rr}\frac{\tau^1}{\sqrt{2}}, \tag{25}$$

$$\log_{10}(\sigma(\tau)) = \log_{10}(\tau) + \log_{10}(\sigma_{rr}) - \log_{10}(\sqrt{2}), \tag{26}$$

which implies σ_{rr} can be identified in an Allan deviation curve by finding a +1 slope when plotting $\log_{10}(\sigma_a(\tau))$ against $\log_{10}(\tau)$. Letting $\tau = \sqrt{2}$ in (26) solves the equation for σ_{rr}, which means if the +1 slope line is projected to $\tau = \sqrt{2}$, the value of $\sigma_a(\tau)$ at that point will equal σ_{rr}.

Although the five sources of error are well defined mathematically along the Allan deviation curve via the use of the slope method, methods for solution are based upon visual inspection of the graph. That is, for a specific sensor and application, lines with the specific slope(s) of interest are created and estimates for each parameter are back-solved by hand or through human-visual inspection. With current autonomous systems, this tedious process hampers efficient calibration of IMU's, especially when the available sensor data are not long enough to ensure a stable Allan variance curve. Although the length of available data required varies with each source of error and its true underlying value, general rules of thumb[4,7] suggest several hours of data are usually required for the slope method to provide accurate estimates of all sources, especially for those prevalent in the latter regions of the τ domain (eg, σ_{rrw} and σ_{rr}) since their effects are only visible after several hours of continuous IMU operation.

3 | AN AUTONOMOUS METHOD FOR ESTIMATING NOISE STRENGTH

The proposed method, referred to as the autonomous regression method for Allan variance (ARMAV) from hereon, differs from the slope method in that it combines linear ridge regression[15] and nonlinear model estimation[16] in order to yield accurate and stable estimates for the five common noise sources in IMU's instead of using visual inspection of graphical methods that are hard to automate. As designed, ARMAV not only performs comparably in terms of estimation accuracy but is also completely autonomous, stable under limited data conditions, and suitable for online IMU characterization.

The key components of the slope method, which are summarized in Table 1, provide the fundamental relationships between observed data (Allan variance) and its predictor variable, τ. However, the slope method identifies each noise strength coefficient individually by restricting the graphical search to the areas of the τ domain where each noise source is dominant. Using IEEE[7] and the assumption of independence among the sources of noise, the combined relationship between total Allan variance, σ_a, and the contributions from each of the sources is given by the following:

$$\log_{10}\left(\sigma_a^2\right) = \log_{10}\left(\sigma_{a_q}^2 + \sigma_{a_{rw}}^2 + \sigma_{a_b}^2 + \sigma_{a_{rrw}}^2 + \sigma_{a_{rr}}^2\right). \tag{27}$$

Next, substituting the relationships from Table 1 yields the following:

$$\begin{aligned}\log_{10}\left(\sigma_a^2\right) = \log_{10}\Bigg[&\left(\sigma_q\sqrt{3}\tau^{-1}\right)^2 + \left(\sigma_{rw}\tau_1^{-1/2}\right)^2 \\ &+ \left(\sigma_b\sqrt{\frac{2\log(2)}{\pi}}\right)^2 + \left(\sigma_{rrw}\frac{1}{\sqrt{3}}\tau^{1/2}\right)^2 + \\ &+ \left(\sigma_{rr}\frac{1}{\sqrt{2}}\tau\right)^2\Bigg]\end{aligned} \tag{28}$$

from which a nonlinear regression problem with N observations of the form:

$$\log_{10}(\mathbf{y}^2) = \log_{10}\left[(\mathbf{X}\boldsymbol{\beta})^2\right] + \boldsymbol{\epsilon}, \tag{29}$$

where

$$\mathbf{y} = \begin{bmatrix}\sigma_{a_1}\\ \vdots \\ \sigma_{a_N}\end{bmatrix}, \tag{30}$$

$$\mathbf{X} = \begin{bmatrix}\sqrt{3}\tau_1^{-1} & \tau_1^{-1/2} & 1 & \frac{1}{\sqrt{3}}\tau_1^{1/2} & \frac{1}{\sqrt{2}}\tau_1 \\ \vdots & \vdots & \vdots & \vdots & \vdots \\ \sqrt{3}\tau_N^{-1} & \tau_N^{-1/2} & 1 & \frac{1}{\sqrt{3}}\tau_N^{1/2} & \frac{1}{\sqrt{2}}\tau_N\end{bmatrix}, \tag{31}$$

$$\boldsymbol{\beta} = \begin{bmatrix}\sigma_q \\ \sigma_{rw} \\ \sigma_b^* \\ \sigma_{rrw} \\ \sigma_{rr}\end{bmatrix}, \tag{32}$$

and

$$\boldsymbol{\epsilon} \sim \mathcal{N}(\mathbf{0}, \Sigma), \tag{33}$$

$$\Sigma = \begin{bmatrix}(\sigma_{a_1}\delta_{a_1})^2 & 0 & \cdots & 0 \\ 0 & (\sigma_{a_2}\delta_{a_2})^2 & \cdots & 0 \\ \vdots & \vdots & \vdots & \vdots \\ 0 & 0 & 0 & (\sigma_{a_N}\delta_{a_N})^2\end{bmatrix} \tag{34}$$

can be constructed and solved using any weighted least-squares nonlinear regression algorithm such as Gauss-Newton[16] or Levenberg-Marquardt.[17] However, since nonlinear regression problems often require an accurate initial guess, $\boldsymbol{\beta}_0$, to converge onto the global minimum,

we first use a linear approximation of (29) to solve the linear model:

$$\underbrace{\begin{bmatrix}\sigma_{a_1}\\ \vdots\\ \sigma_{a_N}\end{bmatrix}}_{\mathbf{y}\in\mathbb{R}^{N\times 1}} = \underbrace{\begin{bmatrix}\sqrt{3}\tau_1^{-1} & \tau_1^{-1/2} & 1 & \frac{1}{\sqrt{3}}\tau_1^{1/2} & \frac{1}{\sqrt{2}}\tau_1\\ \vdots & \vdots & \vdots & \vdots & \vdots\\ \sqrt{3}\tau_N^{-1} & \tau_N^{-1/2} & 1 & \frac{1}{\sqrt{3}}\tau_N^{1/2} & \frac{1}{\sqrt{2}}\tau_N\end{bmatrix}}_{\mathbf{X}\in\mathbb{R}^{N\times 5}} \underbrace{\begin{bmatrix}\sigma_{q_0}\\ \sigma_{rw_0}\\ \sigma^*_{b_0}\\ \sigma_{rrw_0}\\ \sigma_{rr_0}\end{bmatrix}}_{\boldsymbol{\beta}_0\in\mathbb{R}^{5\times 1}} + \boldsymbol{\epsilon}. \tag{35}$$

The model described in (35), however, presents a significant multicollinearity problem since almost every column in $\mathbf{X}$ is dependent on τ. Although multicollinearity is usually not a problem when evaluating the model's ability to predict the observed data, it is extremely problematic here since the desired inference (ie, the initial guess) is based on the individual coefficient values in $\boldsymbol{\beta}$. Therefore, ridge regression[15] is used to solve (35) using the following:

$$\hat{\boldsymbol{\beta}}_0 = \left(\mathbf{X}^{\mathrm{T}}\mathbf{X} + \lambda\mathbf{I}\right)^{-1}\mathbf{X}^{\mathrm{T}}\mathbf{y}, \tag{36}$$

where λ is a tunable, small biasing constant. Using the initial guess $\hat{\boldsymbol{\beta}}_0$, the nonlinear model (29) is then solved to produce $\hat{\boldsymbol{\beta}}$. Finally, it is important to realize the desired estimate of σ_b is not directly given by $\hat{\sigma}^*_b$ since it is simply an estimate of the model's intercept. To obtain the desired $\hat{\sigma_b}$, the fitted model in (29) is used along with (22) to yield the following:

$$\hat{\sigma}_b = \sqrt{\frac{\pi}{2\log(2)}}\min\left(\mathbf{X}\hat{\boldsymbol{\beta}}\right). \tag{37}$$

This process is summarized in Algorithm 1. The ARMAV method was validated using a series of Monte-Carlo simulations along with real-world sensor data from a STIM-300 (tactical grade) IMU, the results of which are discussed in the following sections.

4 | SIMULATION

A 3000-trial Monte-Carlo simulation was executed across 30 unique levels where the length of available sensor data was incrementally decreased from 6 hours (5.4 million samples) to 6 minutes (90 000 samples). Using simulated IMU data, both the slope method and ARMAV (Algorithm 1) were used to estimate the five known simulated noise strength coefficients. The true coefficients were fixed for the entire simulation and are summarized in Table 2. Simulated IMU data were generated using the numerical methods described by Jurado and Raquet[18] and are summarized in the following paragraph for completeness.

In general, simulated IMU data were generated as rate signals, with units of [deg/s] or [m/s/s], by applying the appropriate arithmetic operation to the underlying random process for each source of noise, and with the corresponding standard deviation from Table 2. For example, angle/velocity random walk (σ_{rw}) data were generated directly as zero-mean White Gaussian Noise (WGN) since a random walk process in the integrated signal, with units [deg] or [m/s], arises from the integration of WGN in the rate signal, which has units [deg/s] or [m/s/s]. Meanwhile,

TABLE 2 Summary of true noise strength coefficients for Monte-Carlo simulation

Noise Source	Value	Units
σ_q	2×10^{-4}	[deg] or [m/s]
σ_{rw}	8×10^{-3}	[deg/$\sqrt{\text{hr}}$] or [m/s/$\sqrt{\text{hr}}$]
σ_b	1×10^{-1}	[deg/hr] or [m/s/hr]
σ_{rrw}	2.00	[deg/hr/$\sqrt{\text{hr}}$] or [m/s/hr/$\sqrt{\text{hr}}$]
σ_{rr}	5.00	[deg/hr/hr] or [m/s/hr/hr]

Algorithm 1 Autonomous Regression Method for Allan Variance

Input: $\boldsymbol{\sigma}_a, \boldsymbol{\tau}$ ▷ Allan deviation data in [hrs]

$\mathbf{X}_1 \leftarrow \begin{bmatrix}\frac{\sqrt{3}}{\tau} & \frac{1}{\sqrt{\tau}} & \mathbf{1} & \frac{\sqrt{\tau}}{\sqrt{3}} & \frac{\tau}{\sqrt{2}}\end{bmatrix}$ ▷ Construct linear regressor matrix

$\boldsymbol{\beta}_0 \leftarrow \left(\mathbf{X}_1^{\mathrm{T}}\mathbf{X}_1 + \lambda\mathbf{I}\right)^{-1}\mathbf{X}_1^{\mathrm{T}}\boldsymbol{\sigma}_a$ ▷ Ridge regression for initial guess

$\mathbf{X}_2 \leftarrow \begin{bmatrix}\frac{3}{\tau^2} & \frac{1}{\tau} & \mathbf{1} & \frac{\tau}{3} & \frac{\tau^2}{2}\end{bmatrix}$ ▷ Construct nonlinear regressor matrix

$f(\mathbf{X}, \boldsymbol{\beta}) \leftarrow \log_{10}(\mathbf{X}\boldsymbol{\beta}^2)$ ▷ Build nonlinear regression function

$w_i \leftarrow \frac{1}{(\sigma_{a_i}\delta_{a_i})^2} \quad i = 1, \ldots, N$ ▷ Create weight vector from percent error formula

$\boldsymbol{\beta}_1 \leftarrow$ `fitnlm`$(\mathbf{X}_2, \log_{10}(\mathbf{a}^2), f, \boldsymbol{\beta}_0, \text{'weights'}, \mathbf{w})$ ▷ Use nonlinear solver to estimate

Output: $\sigma_q, \sigma_{rw}, \sigma_b, \sigma_{rrw}, \sigma_{rr}$

$\sigma_q \leftarrow \boldsymbol{\beta}_1(1)$ ▷ Extract quantization noise coefficient

$\sigma_{rw} \leftarrow \boldsymbol{\beta}_1(2)$ ▷ Extract random walk noise coefficient

$\sigma_b \leftarrow \sqrt{\frac{\pi}{2\log(2)}}\min\left(\mathbf{X}_1\boldsymbol{\beta}_1\right)$ ▷ Extract bias instability noise coefficient

$\sigma_{rrw} \leftarrow \boldsymbol{\beta}_1(4)$ ▷ Extract rate random walk noise coefficient

$\sigma_{rr} \leftarrow \boldsymbol{\beta}_1(5)$ ▷ Extract rate ramp noise coefficient

rate random walk (σ_{rrw}) data were generated by numerically integrating a WGN sequence, with units [deg/s/s] or [m/s/s/s], since the desired random walk was to be found in the rate signal and not its integral.

Next, the ARMAV method was programmed as shown in Algorithm 1, with a $\lambda = 5 \times 10^{-3}$ value. The particular λ value was found experimentally by monitoring variation inflation factor (VIF) values.[19] It is important to note that the specific value of λ did not have a significant effect on the final coefficient estimates since it only affected the initial guess used in nonlinear regression.

Finally, the slope method was programmed for comparison to ARMAV also using the methods described by Jurado and Raquet.[18] As a brief summary, the slope method was programmed to calculate the slope of the observed Allan deviation data and find the closest point (Euclidean distance) on the slope curve to each of the five slopes of interest. Then, the Allan deviation value at the particular τ of interest was found by using a point-slope formula for the desired line.

For each of the 30 distinct levels of available sensor data, 3000 trials were conducted, and the resulting mean relative bias and associated 95% basic percentile confidence intervals were estimated by bootstrapping. Figure 3 illustrates the percent relative mean bias and associated 95% basic percentile confidence interval for each level of the simulation and for each of the five noise sources, all relative to their respective true values from Table 2. Additionally, Table 3 summarizes percent relative bias results from the simulation at the 1-hour, 3-hour, and 6-hour levels.

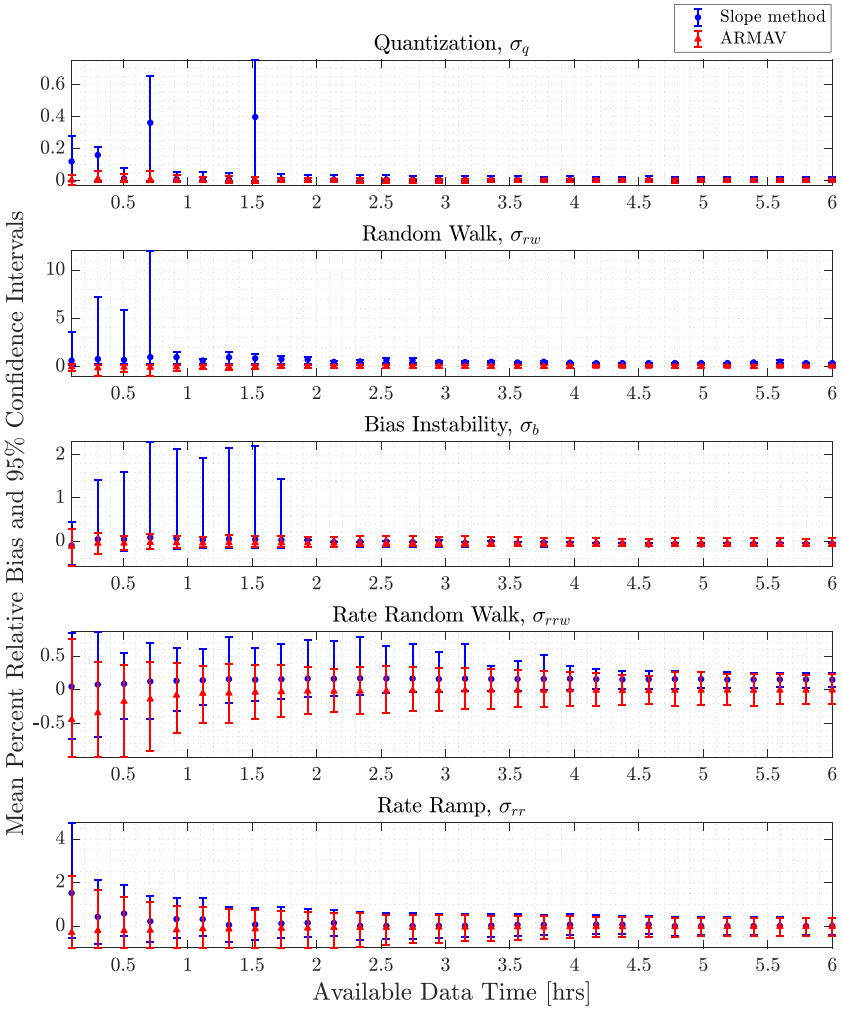

FIGURE 3 Monte-Carlo comparison between slope and regression method. The ARMAV method produced significantly more accurate, and stable results (in terms of variance) as indicated by the confidence intervals, especially as the length of available data decreased below 2 hours [Color figure can be viewed at wileyonlinelibrary.com and www.ion.org]

Overall, both the figure and the table illustrate more stable and generally more accurate estimates when using ARMAV, especially when the length of available data is greater than one hour. As shown in both Figure 3 and Table 3, ARMAV produced substantially more stable results (in terms of variance) as indicated by the width of the confidence interval, especially as the length of available data decreased below two hours. With the exception of σ_{rrw}, percent relative bias was smaller with less variability when ARMAV was used to estimate the errors than when the slope method was used. In the case of σ_{rrw}, ARMAV resulted in a lower percent relative bias until the length of available data fell below 30 minutes. It is also important to note that the slope method resulted in several instances of large variance for particular lengths of available data, generally less than 2 hours, across every noise source.

Comparisons of resulting estimation of ARMAV to the slope method were also conducted for applications and settings in which the Allan deviation curve is essentially incomplete. In these scenarios, the simulated stochastic processes did not include one of the five common noise

TABLE 3 Mean percent relative bias comparison between ARMAV and slope method

		Slope Method				Regression Method			
Time	$\hat{\beta}$	**Mean**	**Std. Dev.**	**95% LCL**	**95% UCL**	**Mean**	**Std. Dev.**	**95% LCL**	**95% UCL**
1 hour	$\hat{\sigma}_q$	1.03×10^{-2}	1.48×10^{-2}	3.02×10^{-4}	5.31×10^{-2}	3.65×10^{-3}	8.26×10^{-3}	8.47×10^{-3}	2.37×10^{-2}
	$\hat{\sigma}_{rw}$	6.15×10^{-1}	2.87	2.93×10^{-1}	4.16×10^{-1}	-2.98×10^{-2}	1.11×10^{-1}	-2.67×10^{-1}	1.26×10^{-1}
	$\hat{\sigma}_b$	2.80×10^{-2}	5.71×10^{-1}	1.65×10^{-1}	1.93	-4.79×10^{-2}	6.18×10^{-2}	-1.48×10^{-1}	1.05×10^{-1}
	$\hat{\sigma}_{rrw}$	1.42×10^{-1}	2.04×10^{-1}	-2.28×10^{-1}	6.00×10^{-1}	-5.42×10^{-2}	2.12×10^{-1}	-4.92×10^{-1}	3.50×10^{-1}
	$\hat{\sigma}_{rr}$	3.16×10^{-1}	4.34×10^{-1}	-4.54×10^{-1}	1.27	-1.26×10^{-1}	5.25×10^{-1}	−1.00	8.57×10^{-1}
3 hours	$\hat{\sigma}_q$	6.38×10^{-3}	8.56×10^{-3}	2.27×10^{-6}	3.04×10^{-2}	9.81×10^{-4}	5.77×10^{-3}	-1.24×10^{-2}	1.17×10^{-2}
	$\hat{\sigma}_{rw}$	4.55×10^{-1}	3.26	3.17×10^{-1}	3.87×10^{-1}	1.78×10^{-3}	7.10×10^{-2}	-1.30×10^{-1}	1.61×10^{-1}
	$\hat{\sigma}_b$	-4.31×10^{-2}	5.81×10^{-1}	-1.29×10^{-1}	-2.88×10^{-2}	-4.64×10^{-2}	5.37×10^{-2}	-1.15×10^{-1}	1.08×10^{-1}
	$\hat{\sigma}_{rrw}$	1.66×10^{-1}	1.86×10^{-1}	-2.02×10^{-2}	6.76×10^{-1}	-6.57×10^{-3}	1.51×10^{-1}	-2.91×10^{-1}	3.26×10^{-1}
	$\hat{\sigma}_{rr}$	1.32×10^{-2}	2.71×10^{-1}	-5.15×10^{-1}	5.41×10^{-1}	-5.72×10^{-2}	2.93×10^{-1}	-6.80×10^{-1}	4.91×10^{-1}
6 hours	$\hat{\sigma}_q$	4.75×10^{-3}	6.09×10^{-3}	1.03×10^{-4}	2.17×10^{-2}	8.32×10^{-4}	4.23×10^{-3}	-9.06×10^{-3}	8.82×10^{-3}
	$\hat{\sigma}_{rw}$	3.53×10^{-1}	1.30×10^{-2}	3.27×10^{-1}	3.78×10^{-1}	4.26×10^{-3}	5.32×10^{-2}	-9.73×10^{-2}	1.37×10^{-1}
	$\hat{\sigma}_b$	-6.32×10^{-2}	5.05×10^{-1}	-1.14×10^{-1}	-4.25×10^{-2}	-5.50×10^{-2}	3.92×10^{-2}	-1.05×10^{-1}	5.96×10^{-2}
	$\hat{\sigma}_{rrw}$	1.50×10^{-1}	1.14×10^{-1}	4.06×10^{-2}	2.47×10^{-1}	-5.18×10^{-3}	1.09×10^{-1}	-2.11×10^{-1}	2.30×10^{-1}
	$\hat{\sigma}_{rr}$	2.45×10^{-3}	2.02×10^{-1}	-4.16×10^{-1}	3.92×10^{-1}	-2.29×10^{-2}	1.95×10^{-1}	-4.35×10^{-1}	3.50×10^{-1}

Abbreviations: LCL, lower confidence level from basic percentile; UCL, upper confidence level from basic percentile.

TABLE 4 Actual estimation bias comparisons between regression and slope methods, no quantization noise

		Slope Method: Auto		Slope Method: Manual		Regression Method	
Time	$\hat{\beta}$	**Mean**	**Std. Dev.**	**Mean**	**Std. Dev**	**Mean**	**Std. Dev.**
1 hr	$\hat{\sigma}_q$	4.25×10^{-3}	1.69×10^{-2}	–	–	6.81×10^{-7}	7.73×10^{-7}
	$\hat{\sigma}_{rw}$	5.60×10^{-5}	1.26×10^{-3}	5.60×10^{-5}	1.26×10^{-3}	1.83×10^{-5}	1.14×10^{-4}
	$\hat{\sigma}_b$	1.39×10^{-1}	1.44×10^{-1}	1.39×10^{-1}	1.44×10^{-1}	1.14×10^{-1}	1.17×10^{-2}
	$\hat{\sigma}_{rrw}$	2.56×10^{-1}	4.38×10^{-1}	2.56×10^{-1}	4.38×10^{-1}	-1.20×10^{-1}	3.77×10^{-1}
	$\hat{\sigma}_{rr}$	1.57	2.33	1.57	2.33	-7.38×10^{-1}	2.80
3 hrs	$\hat{\sigma}_q$	1.40×10^{-3}	3.13×10^{-2}	–	–	3.37×10^{-7}	5.07×10^{-7}
	$\hat{\sigma}_{rw}$	2.45×10^{-5}	4.64×10^{-5}	2.45×10^{-5}	4.64×10^{-5}	4.56×10^{-5}	6.08×10^{-5}
	$\hat{\sigma}_b$	1.19×10^{-1}	1.49×10^{-1}	1.19×10^{-1}	1.49×10^{-1}	1.13×10^{-1}	6.60×10^{-3}
	$\hat{\sigma}_{rrw}$	3.14×10^{-1}	3.30×10^{-1}	3.14×10^{-1}	3.30×10^{-1}	-2.41×10^{-2}	2.17×10^{-1}
	$\hat{\sigma}_{rr}$	2.66×10^{-1}	1.27	2.66×10^{-1}	1.27	-1.96×10^{-1}	1.34
6 hrs	$\hat{\sigma}_q$	7.71×10^{-5}	4.07×10^{-5}	–	–	2.40×10^{-7}	4.08×10^{-7}
	$\hat{\sigma}_{rw}$	2.27×10^{-5}	4.25×10^{-5}	2.27×10^{-5}	4.25×10^{-5}	4.53×10^{-5}	4.89×10^{-5}
	$\hat{\sigma}_b$	1.09×10^{-1}	4.08×10^{-3}	1.09×10^{-1}	4.08×10^{-3}	1.12×10^{-1}	5.04×10^{-3}
	$\hat{\sigma}_{rrw}$	2.91×10^{-1}	2.10×10^{-1}	2.91×10^{-1}	2.10×10^{-1}	-2.09×10^{-2}	1.68×10^{-1}
	$\hat{\sigma}_{rr}$	3.94×10^{-2}	1.02	3.94×10^{-2}	1.02	-6.97×10^{-2}	9.73×10^{-1}

components, ie, either quantization or rate ramp components was not included in the simulated IMU data. In these comparisons, another set of 3000-trial Monte-Carlo simulations were conducted separately for each source of error and in the same manner as previously presented, with the exception that the true σ_q and σ_{rr} were set to zero in each simulation, respectively. For comparison, results from the slope method were also computed using two techniques: In autonomous mode, the slope method was allowed to run as previously described[18] with no additional human intervention, while in manual mode, the slope method was reprogrammed to skip the estimation of the particular noise coefficient that was known to be zero. Tables 4 and 5 provide, respectively, the results of these simulations for the cases when quantization and rate ramp components were missing. Results are presented in terms of bias rather than percent relative bias for better comparisons.

As shown in both tables, the nonnormalized biases from ARMAV were up to four orders of magnitude closer to the truth (zero) when compared with the autonomous slope method. This is due to the fact the slope method, when programmed, looks for all parameters (ie, finds the closest answer matching the graphical method for each noise coefficient). In contrast, the manual slope method was reprogrammed to assume the missing noise coefficient was zero. As expected, its results for all other coefficients were an exact match to the autonomous-mode slope method. Here, it is important to emphasize these scenarios had to be specially programmed from an initial visual inspection of the Allan variance data for the slope method to produce good results. In contrast, for data applications in which these sources of noise are not estimable from the data, ARMAV autonomously and reliably provided reasonable estimates with no changes to the programmed algorithm.

5 | APPLICATION TO STIM-300 IMU ANALYSIS

The ARMAV method was applied to real-world sensor data from an STIM-300 (tactical grade) IMU. The manufac-

TABLE 5 Actual estimation bias comparisons bewteen regression and slope method, no rate ramp noise

		Slope Method: Auto		Slope Method: Manual		Regression Method	
Time	$\hat{\beta}$	**Mean**	**Std. Dev.**	**Mean**	**Std. Dev.**	**Mean**	**Std. Dev.**
1 hr	$\hat{\sigma}_q$	5.04×10^{-5}	1.56×10^{-3}	5.04×10^{-5}	1.56×10^{-3}	2.94×10^{-6}	3.46×10^{-6}
	$\hat{\sigma}_{rw}$	1.28×10^{-2}	4.32×10^{-2}	1.28×10^{-2}	4.32×10^{-2}	-1.43×10^{-3}	2.06×10^{-3}
	$\hat{\sigma}_b$	1.83×10^{-1}	1.69×10^{-1}	1.83×10^{-1}	1.69×10^{-1}	1.28×10^{-1}	1.78×10^{-2}
	$\hat{\sigma}_{rrw}$	-9.21×10^{-2}	4.76×10^{-1}	-9.21×10^{-2}	4.76×10^{-1}	-3.77×10^{-1}	4.90×10^{-1}
	$\hat{\sigma}_{rr}$	5.28	2.85	–	–	1.17	1.66
3 hrs	$\hat{\sigma}_q$	5.42×10^{-4}	1.73×10^{-2}	5.42×10^{-4}	1.73×10^{-2}	2.22×10^{-6}	2.86×10^{-6}
	$\hat{\sigma}_{rw}$	3.70×10^{-2}	1.57×10^{-1}	3.70×10^{-2}	1.57×10^{-1}	-9.57×10^{-4}	1.47×10^{-3}
	$\hat{\sigma}_b$	2.60×10^{-1}	3.62×10^{-1}	2.60×10^{-1}	3.62×10^{-1}	1.28×10^{-1}	1.30×10^{-2}
	$\hat{\sigma}_{rrw}$	-8.31×10^{-2}	3.69×10^{-1}	-8.31×10^{-2}	3.69×10^{-1}	-1.90×10^{-1}	3.06×10^{-1}
	$\hat{\sigma}_{rr}$	3.04	2.08	–	–	5.43×10^{-1}	8.31×10^{-1}
6 hrs	$\hat{\sigma}_q$	9.36×10^{-4}	2.87×10^{-2}	9.36×10^{-4}	2.87×10^{-2}	2.01×10^{-6}	2.60×10^{-6}
	$\hat{\sigma}_{rw}$	6.83×10^{-2}	3.06×10^{-1}	6.83×10^{-2}	3.06×10^{-1}	-7.79×10^{-4}	1.23×10^{-3}
	$\hat{\sigma}_b$	3.25×10^{-1}	5.28×10^{-1}	3.25×10^{-1}	5.28×10^{-1}	1.29×10^{-1}	1.23×10^{-2}
	$\hat{\sigma}_{rrw}$	-6.79×10^{-2}	3.53×10^{-1}	-6.79×10^{-2}	3.53×10^{-1}	-1.53×10^{-1}	2.69×10^{-1}
	$\hat{\sigma}_{rr}$	2.17	1.78	–	–	4.02×10^{-1}	6.32×10^{-1}

TABLE 6 Summary of Allan variance analysis results for STIM-300 IMU sensors

	Accelerometer				Gyroscope			
$\hat{\beta}$	**Slope: Auto**	**Slope:Manual**	**Regression**	**Spec**	**Slope: Auto**	**Slope: Manual**	**Regression**	**Spec**
$\hat{\sigma}_q$	7.44×10^{-5}	–	7.28×10^{-1}	–	1.61×10^{-2}	–	3.28×10^{-5}	–
$\hat{\sigma}_{rw}$	5.08×10^{-2}	5.08×10^{-2}	5.41×10^{-2}	6.00×10^{-2}	1.51×10^{-1}	1.51×10^{-1}	1.51×10^{-1}	1.50×10^{-1}
$\hat{\sigma}_b$	2.99	2.99	2.99	2.66	6.66×10^{-1}	6.66×10^{-1}	6.75×10^{-1}	5.00×10^{-1}
$\hat{\sigma}_{rrw}$	3.79×10^{1}	3.79×10^{1}	3.84×10^{1}	–	1.33	1.33	9.00×10^{-1}	–
$\hat{\sigma}_{rr}$	4.28×10^{1}	4.28×10^{1}	4.73×10^{1}	–	9.85×10^{-1}	9.85×10^{-1}	8.45×10^{-1}	–

turer of this sensor provides specifications for the values of σ_{rw} and σ_b,[20] which are reproduced along with the analysis results in Table 6. A single 6-hour data collection was performed at static conditions and room temperature for the x-axis accelerometer and gyroscope at a sampling rate of 250 Hz. It is important to note that the purpose of this data collection was to simply demonstrate the ability of ARMAV to match manufacturer specifications, which were only specified for the random walk and bias instability components. Therefore, the internal temperature of the IMU was not tightly controlled. The MATLAB code and inertial dataset used in this research are provided as supplementary materials via Autonomous Regression Method for Allan Variance.[21] Plots of the fitted Allan deviance curve resulting from the application of the regression method for both the accelerometer and gyroscope are provided in Figures 4 and 5. As shown, ARMAV is able to accurately model the observed data from both devices with no need for human intervention and directly enables the accurate estimation of the necessary noise strength coefficients. The resulting 95% prediction bands generated in each figure cover the possible range of future observations simultaneously and provide a measure of the model's quality. Finally, Table 6 provides the results from ARMAV on the STIM-300 IMU data and compares these estimates to the slope method. As shown, the particular sensor tested did not exhibit quantization noise (ie, $\sigma_q = 0$), yet ARMAV was able to accurately estimate all noise coefficients, and in the case of σ_q, its estimates were up to five orders of magnitude closer to zero when compared with the autonomous slope method. Additionally, in the case of σ_{rw} and σ_b, where the manufacturer provided specifications,[20] ARMAV was closer to specifications in the majority of cases and always at least as accurate as the slope method.

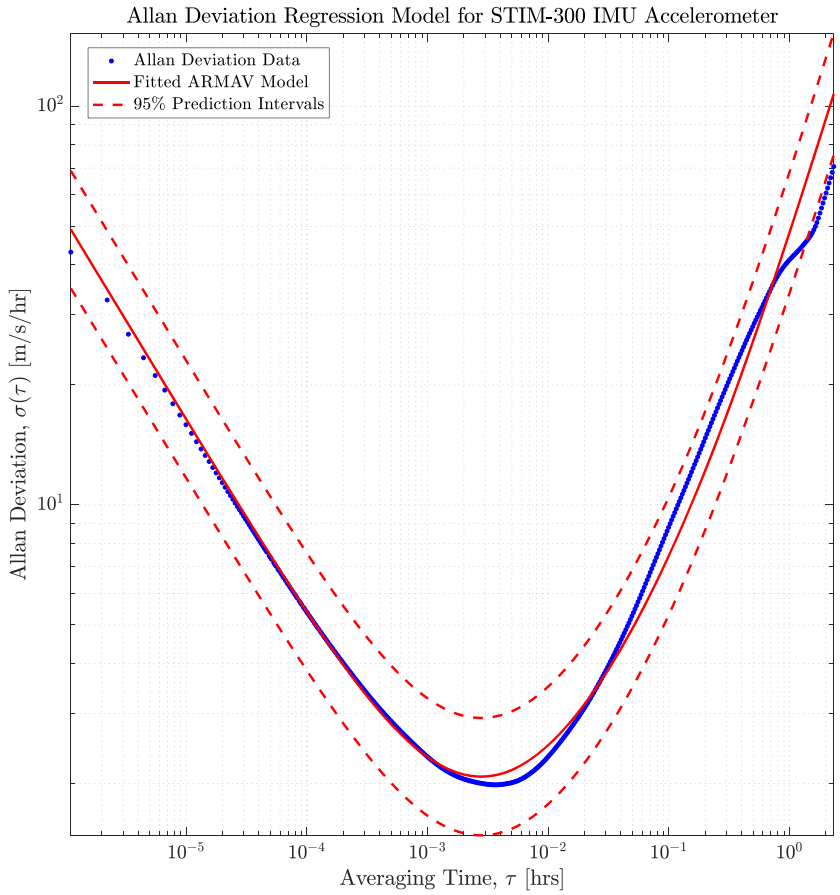

FIGURE 4 Illustration of fitted nonlinear model on accelerometer Allan deviation measurements. As shown, ARMAV is able to accurately model the observed data with no need for human intervention, directly enabling the accurate estimation of the necessary noise strength coefficients. The resulting 95% prediction intervals cover a possible range of Allan deviation observations for each τ [Color figure can be viewed at wileyonlinelibrary.com and www.ion.org]

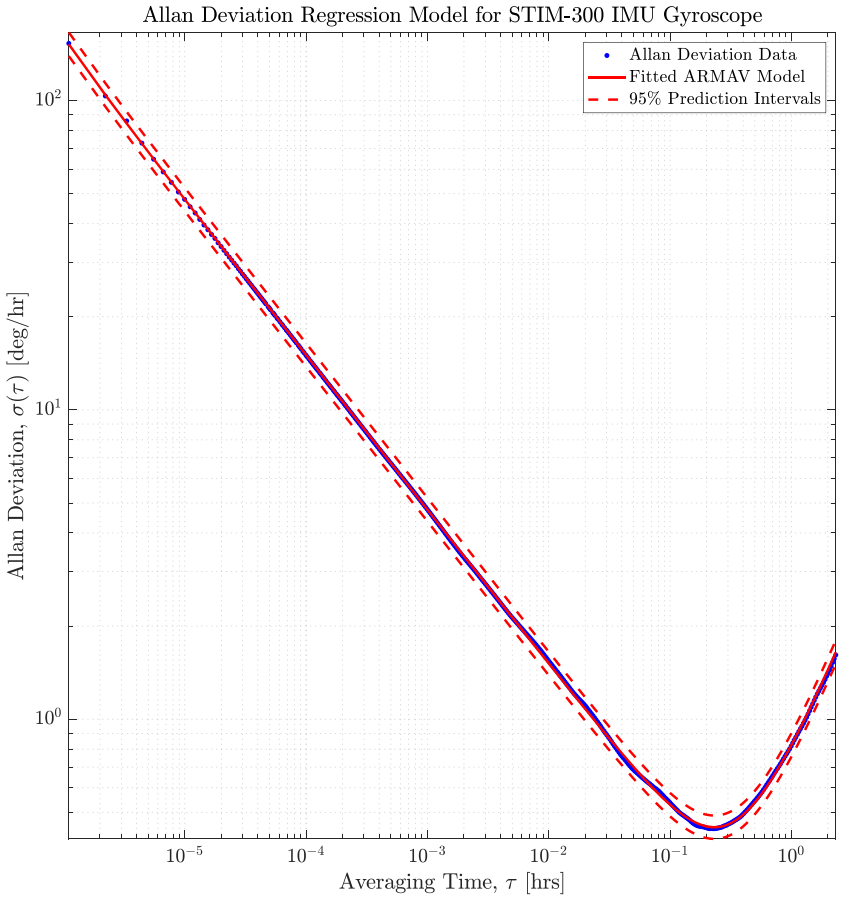

FIGURE 5 Illustration of fitted nonlinear model on gyroscope Allan deviation measurements. As shown, ARMAV is able to accurately model the observed data with no need for human intervention, directly enabling the accurate estimation of the necessary noise strength coefficients. The resulting 95% prediction intervals cover a possible range of Allan deviation observations for each τ [Color figure can be viewed at wileyonlinelibrary.com and www.ion.org]

6 | CONCLUSIONS AND FUTURE WORK

This research has proposed a novel autonomous, regression-based method for the Allan variance analysis, in the context of IMU sensor calibration. The ARMAV method was shown to be generally more accurate and stable than the state-of-the-art slope method, especially when the length of available sensor data was greater than one hour. Additionally, ARMAV was shown to be completely autonomous and simple to program, requiring no further human input even when particular sources of noise were not present in the observed data. These findings provide significant advances in the calibration of inertial sensors as the state-of-the art method (the slope method) requires human input either via visual inspection of Allan deviance curves, or specific coding that is not transferable to other observed or updated data sets. As such, this method directly enables online or autonomous IMU sensor calibration using the Allan variance, with no prior knowledge on the specific sources of noise affecting an inertial sensor of interest. Future work in this area involves the integration of the ARMAV method into an online navigation framework, where a navigation computer is able to constantly update its internal IMU model based on Allan variance analysis of observed IMU output. The implications of this integration is a continually updated, safe, accurate awareness of vehicle position, velocity, and orientation at all times.

DISCLAIMER

The views expressed in this paper are those of the authors and do not reflect the official policy or position of the United States Air Force, Department of Defense, or the U.S. Government.

ORCID

Juan Jurado https://orcid.org/0000-0003-3600-6239

REFERENCES

1. Titterton D, Weston J. *Strapdown Inertial Navigation Technology*. Second Edition, Vol. 207. US: AIAA; 2005.
2. Allan DW. Statistics of atomic frequency standards. *Proceedings of the IEEE*. Feb 1966;54(2):221-230.
3. Kirkko-Jaakkola M, Collin J, Takala J. Bias prediction for MEMS gyroscopes. *IEEE Sensors J*. June 2012;12(6):2157-2163.
4. Hou H. Modeling inertial sensor errors using allan variance. *Master's Thesis*: University of Calgary, Calgary, Canada; September 2004.
5. El-Sheimy N, Hou N, Niu X. Analysis and modeling of inertial sensors using allan variance. *IEEE Transac Instrumentation Meas*. 2008;57(1):140-149.
6. Allan Variance: Noise Analysis for Gyroscopes. https://doi.org/cache.freescale.com/files/sensors/doc/app_note/AN5087.pdf; 2015.
7. IEEE. IEEE standard specification format guide and test procedure for single-axis interferometric fiber optic gyros. IEEE Std 952-1997; 1998.
8. Stebler Y, Guerrier S, Skaloud J, Victoria-Feser M-P. Generalized method of wavelet moments for inertial navigation filter design. *IEEE Transac Aerospace Electronic Syst*. 2014;50(3):2269-2283.
9. Radi A, Bakalli G, El-Sheimy N, Guerrier S, Molinari R. An automatic calibration approach for the stochastic parameters of inertial sensors. *Proceedings of the 30th International Technical Meeting of The Satellite Division of the Institute of Navigation (ION GNSS+2017);* Portland, OR, USA; September 2017; 3053-3060.
10. Guerrier S, Skaloud J, Stebler Y, Victoria-Feser M-P. Wavelet-variance-based estimation for composite stochastic processes. *J American Stat Assoc*. 2013;108(503):1021-1030.
11. Papoulis A, Pillai SU. *Probability, Random Variables, and Stochastic Processes*. New York, USA: McGaw-Hill; 1991.
12. Bennett WR. Spectra of quantized signals. *Bell Syst Tech J*. 1948;27(3):446-472.
13. Kalman RE. A new approach to linear filtering and prediction problems. *J Basic Eng*. 1960;82(1):35-45.
14. Maybeck PS. *Stochastic Models, Estimation, and Control*, Vol. 1. Virginia: Navtech; 1982.
15. Hoerl AE, Kennard RW. Ridge regression: biased estimation for nonorthogonal problems. *Technometrics*. 1970;12(1):55-67.
16. Bates DM, Watts DG. *Nonlinear Regression Analysis and Its Applications*, Wiley series in probability and mathematical statistics. Applied probability and statistics. New York, Chichester: J. Wiley; 1988. Includes indexes.
17. Marquardt DW. An algorithm for least-squares estimation of nonlinear parameters. *J Soc Indust Appl Math*. 1963;11(2):431-441.
18. Jurado J, Raquet J. A common framework for inertial sensor error modeling. *Proceedings of the ION Pacific PNT*, Honolulu, HI, USA, May 2017;725-740.
19. Kutner MH, Nachtsheim C, Neter J. *Applied Linear Regression Models*, Vol. 4. New York: McGraw-Hill/Irwin; 2004.
20. STIM 300 Inertial Measurement Unit Datasheet. http://www.sensonor.com/media/91313/ts1524.r8%20datasheet%20stim300.pdf; April 2013.
21. Autonomous Regression Method for Allan Variance. https://doi.org/www.mathworks.com/matlabcentral/fileexchange/66462-autonomous-regression-method-for-allan-variance; 2018.

How to cite this article: Jurado J, Schubert Kabban CM, Raquet J. A regression-based methodology to improve estimation of inertial sensor errors using Allan variance data. *NAVIGATION*. 2019;1–13. https://doi.org/10.1002/navi.278